HAL open science

A coupled rotor dynamic simulation of an electric drive train to investigate the acoustic behavior

Sebastian Koch, Fabian Duvigneau, Elmar Woschke

To cite this version:

Sebastian Koch, Fabian Duvigneau, Elmar Woschke. A coupled rotor dynamic simulation of an electric drive train to investigate the acoustic behavior. eForum Acusticum 2020, Dec 2020, Lyon, France. pp.2945-2950, 10.48465/fa.2020.0371 . hal-03229461

HAL Id: hal-03229461

https://hal.science/hal-03229461v1

Submitted on 21 May 2021

HAL is a multi-disciplinary open access archive for the deposit and dissemination of scientific research documents, whether they are published or not. The documents may come from teaching and research institutions in France or abroad, or from public or private research centers.

L'archive ouverte pluridisciplinaire **HAL**, est destinée au dépôt et à la diffusion de documents scientifiques de niveau recherche, publiés ou non, émanant des établissements d'enseignement et de recherche français ou étrangers, des laboratoires publics ou privés.

A COUPLED ROTOR DYNAMIC SIMULATION OF AN ELECTRIC DRIVE TRAIN TO INVESTIGATE THE ACOUSTIC BEHAVIOR

Sebastian Koch[1] **Fabian Duvigneau**[1] **Elmar Woschke**[1]

[1] Institute of Mechanics, Otto von Guericke University Magdeburg , Germany
sebastian.koch@ovgu.de, fabian.duvigneau@ovgu.de, elmar.woschke@ovgu.de

ABSTRACT

In order to improve the acoustic behavior of an electric drive train a holistic simulation approach is presented that considers the interactions of structural mechanics and electrodynamics. The electrodynamic forces in the motor influence both the rotor dynamics and the structure vibration and thus the sound radiation. Even small variations of the air gap lead to changes in the electrodynamic field, which cause a change in the resulting loads and therefore vibration excitation. Especially air gap changes due to load- and operation-dependent deformations of the stator and rotor are problematic. Such deformations influence the electrodynamically excited structural vibrations as well as the rotordynamic loads. Therefore, it is necessary to consider the electro- and structural-dynamic effects together. In this study, the finite element method (FEM) is used to calculate both the deformation of the structure and the electrodynamic forces. The forces determined using the FEM, for instance as a function of the current rotor eccentricity, are used as excitation in a multi-body simulation (MBS) and thus allow the description of the structural vibrations, whereby bearings such as ball bearings or hydrodynamic bearings can be taken into account. In addition the sound radiation of the vibrating structures is studied. Subsequently, design measures can be evaluated based on possible improvements by means of parameter studies, without the necessity of real prototypes. Due to the general simulation approach, the presented methodology is not limited to the investigated engine.

1. INTRODUCTION

The emitted noise is a central problem of all electrical machines. Mainly due to the fact that the typical sound emission of an electric motor is very tonal and contains higher frequencies, noise of electric machines is perceived as particularly annoying. For this reason, the numerical analysis of sound radiation is an important tool to be able to predict the acoustic behavior at an early stage of the product development process. It should be noted that smallest variations in the air gap of the motor can change the electromagnetic fields and the resulting forces and moments. An eccentric rotor creates a strong force in the direction of the smallest air gap between rotor and stator [1]. This force is called unbalanced magnetic pull (UMP) and influences the vibration behavior of the structure [2], which influences the air gap, and the acoustics of the system as well. These days, the interactions between mechanical structure and electromagnetic components are usually not taken into account. In contrast, a coupled approach including the feedback of the interactions of structural vibrations and electrodynamics is presented in this paper. Especially, in the context of rotor dynamic analysis the coupling of electrodynamics and multi body systems is novel. The need for such a holistic simulation approach that considers these interactions arised in a previous study of an electric wheel hub motor [3].

2. THEORETICAL BASICS

2.1 Multi body simulation of mechanical systems

Multi body simulations are used to describes the spatial motion and dynamic behavior of bodies effected by arbitrary loads which can also include electrodynamic forces. In general the interactions between different bodies, which can be modeled either as ideal rigid or elastic deformable, determine the dynamical behaviour of the overall system. These interactions can be described using defined force laws or alternatively by constraint equations (for example in the case of joints).

Starting from the linear momentum and angular momentum for rigid bodies or using a mechanical principle (e.g. Hamilton's principle) for the description of elastic bodies, the resulting equation of motion of the multi body system can be derived [4, 5]

$$\underline{\underline{M}}_{\text{MBS}}(\underline{q},\underline{\dot{q}})\,\underline{\ddot{y}} + \underline{h}_{\omega}(\underline{\omega},\underline{q},\underline{\dot{q}}) + \underline{h}_{\text{el}}(\underline{q},\underline{\dot{q}}) = h_{\text{o}}(\underline{x},\underline{\dot{x}},\underline{\varphi},\underline{\omega},\underline{q},\underline{\dot{q}},t) \quad . \tag{1}$$

For calculation of the kinematic quantities position $\underline{x}$, orientation $\underline{\varphi}$ and elastic deformations $\underline{q}$ as well as their time derivatives, the inertia terms, which are represented by the mass matrix $\underline{\underline{M}}_{\text{MBS}}$ and the accelaration vector $\underline{\ddot{y}} = [\underline{\ddot{x}}\ \underline{\dot{\omega}}\ \underline{\ddot{q}}]^T$, the vector of centrifugal-, coriolis- and gyroscopic forces $\underline{h}_{\omega}$, the elastic characteristics represented by the vector of elastic forces $\underline{h}_{\text{el}}$ and the acting forces have to be considered. After transformation into state space without taking into account constraint equations

$$\underline{z} = [\underline{y}\ \ \underline{\dot{y}}]^T \tag{2}$$

the resulting ordinary differential equation (ODE)

$$\underline{\dot{z}} = \underline{\Phi}(\underline{z}) = [\underline{\dot{y}} \quad \underline{\underline{M}}^{-1}_{\text{MBS}}(\underline{h}_{\text{o}} - \underline{h}_{\omega} - \underline{h}_{\text{el}})]^T \tag{3}$$

can be solved by standardized ODE solvers. Due to the rather stiff numerical behaviour as a result of the electrodynamic forces, which are included in the vector of outer forces $\underline{h}_{\mathrm{o}}$, a two-level implicit Runge-Kutta method based on the trapezoidal rule is used in this paper, also known as ODE23t.

2.2 Finite element analyses of electromagnetic fields

The finite element method (FEM) is a numerical method for solving differential equations and is widely used in engineering problems. Its use for the formulation of electrodynamic phenomena is described in detail in various literature [6–8], leading to the following system of equations

$$\underline{\underline{K}}\,\underline{A} = \underline{J} + \underline{B}_0 \tag{4}$$

with the permeability matrix $\underline{\underline{K}}$, the magnetic vector potential $\underline{A}$, the current density $\underline{J}$ and the magnetization $\underline{B}_0$. To take eddy currents into account, the system of equations can be expanded by including the conductivity matrix $\underline{\underline{L}}$ and a motion matrix $\underline{\underline{V}}$

$$\underline{\underline{L}}\,\dot{\underline{A}} + (\underline{\underline{V}} + \underline{\underline{K}})\underline{A} = \underline{J} + \underline{B}_0 \quad . \tag{5}$$

The magnetic vector potential $\underline{A}$ is a mathematical auxiliary variable from which the magnetic flux density $\underline{B}$ and the magnetic field intensity $\underline{H}$ can be determined using the magnetic permeability μ and the rotation rot

$$\underline{B} = rot(\underline{A}) \quad , \tag{6}$$

$$\underline{H} = \frac{1}{\mu}\underline{B} \quad . \tag{7}$$

With the magnetic field intensity $\underline{H}$ the electrodynamic forces $\underline{h}_{\mathrm{o,elec}}$ can be calculated and applied as a part of the outer loads $\underline{h}_{\mathrm{o}} = \underline{h}_{\mathrm{o,mech}} + \underline{h}_{\mathrm{o,elec}}$ to the mechanical field problem (MBS procedure). The electrodynamic forces $\underline{h}_{\mathrm{o,elec}}$ are obtained using the Maxwell's stress tensor by an integration along the edges Γ of the element

$$d\underline{h}_{\mathrm{o,elec}} = -\frac{\mu_0}{2}\underline{H}^2 d\Gamma + \mu_0(\underline{H}\cdot d\Gamma)\underline{H} \quad , \tag{8}$$

therein μ_0 is the magnetic permeability. In this paper finite elements with quadratic shape functions are used. In order to improve the convergence and thus reduce the computing time, high order element ansatz functions are aimed for in further works. As shown in Figure 1, higher order elements have a better convergence rate and are also robust against element distortion [9].

2.3 Coupling of structural mechanics and electrodynamics in the context of electric machines

For considering the electrodynamic influences on the mechanical system, an existing multi-body program EMD, developed at the Otto von Guericke University Magdeburg, is extended in order to solve the coupled electromechanical problem dynamically. As it can be seen in Figure 2, the

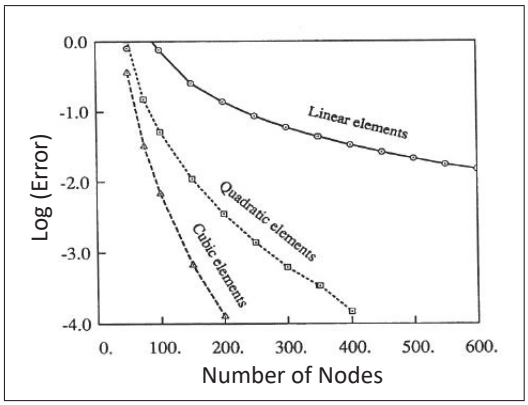

Figure 1. Optimal convergence rates of elements with shape functions of different polynomial order [9].

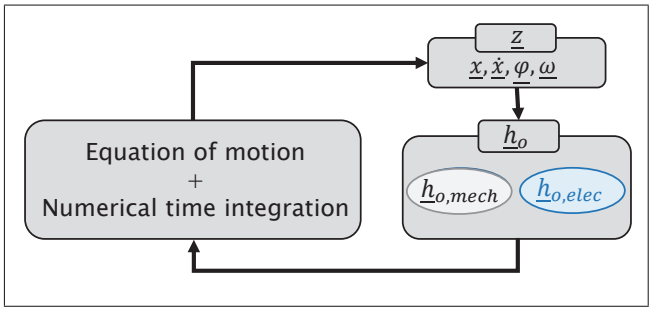

Figure 2. Presented simulation workflow including the coupling between a multi body simulation and an electrodynamic finite element analysis in order to take into account electrodynamic loads (blue).

solution of the electrodynamic problem is done in every time step. The resulting forces are functions of the kinematic quantities such as shaft displacements $\underline{x}$, the corresponding velocities $\dot{\underline{x}}$, the rotational speed $\underline{\omega}$ and the angle of rotation $\underline{\varphi}$. Furthermore, the actual phase of the current and the solution from the last time step are required. In this way, the electrodynamic calculation takes into account the the air gap change of the engine and the MBS considers the changed magnetic forces. Such a coupling including the feedbacks is novel and not implemented in any commercial software until now. With the help of a transient simulation, the vibration behavior of the system can be described considering the mentioned interactions.

3. INVESTIGATION OF THE VIBROACOUSTIC BEHAVIOR OF AN ELECTRIC ENGINE

3.1 Design of the electric engine

The lightweight alternating current motor using an air gap winding shown in Figure 3 is used for the investigations in this paper. It was developed at the Otto von Guericke University Magdeburg, which gives access to a parameterized model and all drawings. In addition, a prototype is available, which can be used for experimental investigations to validate the presented method. The motor has 14 pole pairs and is operated with a current up to 300 A. This external rotor motor was developed as a drive for a

speedboat and is therefore called further on boat motor. It has a maximum torque of 50 Nm, a maximum rotational speed of 3000 rpm, a length of approximately 220 mm and a diameter of roughly 160 mm.

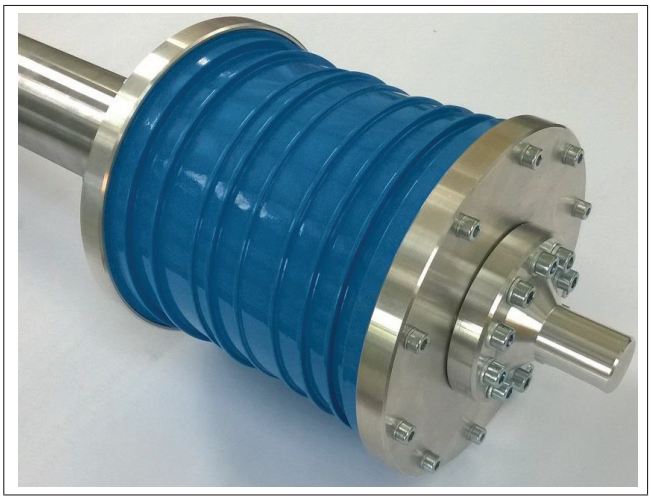

Figure 3. Examined electric motor (an external rotor motor with air gap winding).

Figure 4 shows a section of the electromagnetically relevant components of the motor with air gap winding. The stator with 36 associated copper windings and the rotor with two magnets (one of fourteen pole pairs) can be seen. The electromagnetic components have a depth of 120 mm. A rectangular current I is applied to the copper conductors of the motor. Figure 5 shows the pathway of the current of the three phases for one rotation.

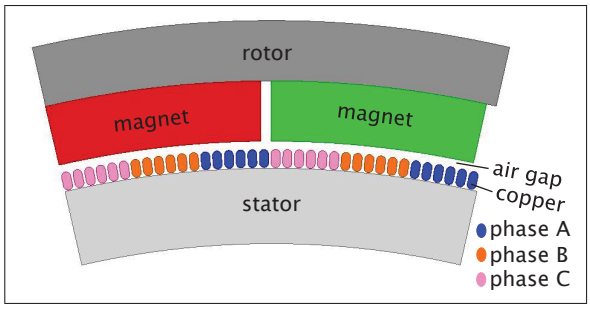

Figure 4. Section of the electromagnetically relevant components of the motor with air gap winding shown in Figure 3.

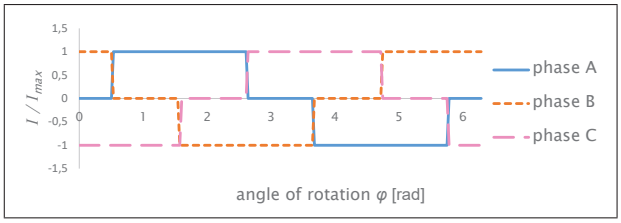

Figure 5. Normalized current I/I_{max} of the three electric phases depending on the angle of rotation φ.

3.2 Vibroacoustic analysis with commercial software

In this chapter the engine shown in section 3.1 is examined by using the commercial software ANSYS. This section is used to verify the simulation results of our own implementation and to look at the steps that are required in the following to determine the acoustic behavior of an electric machine. As already said, it is not possible to consider a coupling including feedback within commercial software. Consequently, only the single parts of the developed holistic simulation approach can be verified by comparison with the results of ANSYS.

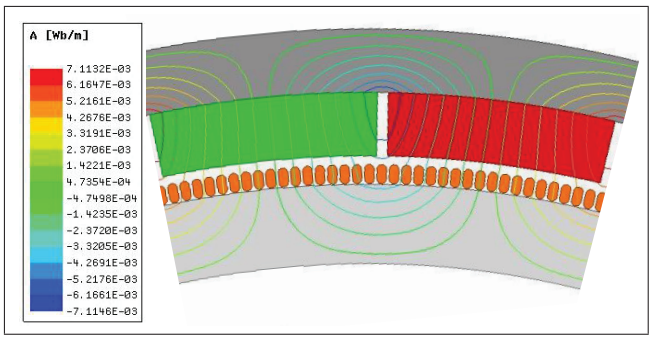

Figure 6. Magnetic vector potential $\underline{A}$ of the boat motor.

In a first step, the electromagnetic fields of the boat motor and the resulting forces and moments are calculated. Figure 6 shows the magnetic vector potential $\underline{A}$, from which the resulting forces and torques can be determined using Maxwell's stress tensor (see equation 8), whereby periodic boundary conditions can be introduced, leading to a significantly smaller system of equations. The calculated torque of 49.6 Nm for an input current of 300 A is in good agreement with experimental results of 47.2 −49.5 Nm (depending on the rotational speed) at 300 A [10]. These forces rotate with the rotational speed and can be used as loads for a harmonic analysis. It is important to note that the motor is always in a central position during the whole analysis. Consequently, the presented coupling of the rotor dynamic and electrodynamic system leads to a more precise approximation of the reality. By neglecting the influence of structural vibration on the air gap, a very efficient calculation is possible. However, an error must be accepted in this case. The resulting structural vibrations of the engine housing for an arbitrary frequency are shown exemplarily in Figure 7. The corresponding sound pressure distribution in the surrounding air can be determined subsequently based on the previously calculated structural vibrations of the surface of the housing of the electric boat motor. Figure 8 shows the sound radiation in a cutting plane in the middle of the spherical air volume, which was determined with an acoustic analysis in an uncoupled manner (no feedback of the air on the structure). On the outer surface of the fluid domain absorbing boundary conditions are used to fulfill the Sommerfeld radiation condition. To ensure a sufficient discretization standard convergence analyses were executed.

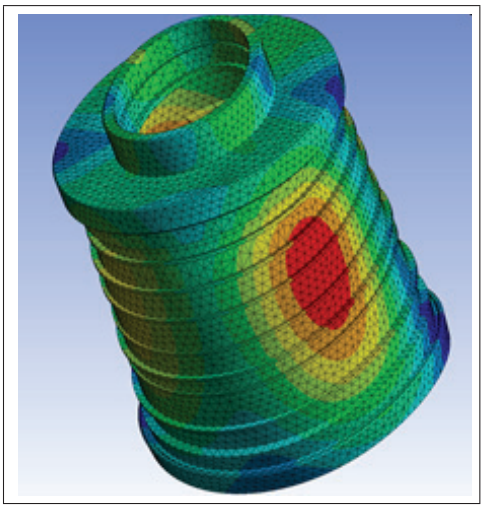

Figure 7. Vibration behavior of the motor housing at an exemplary frequency.

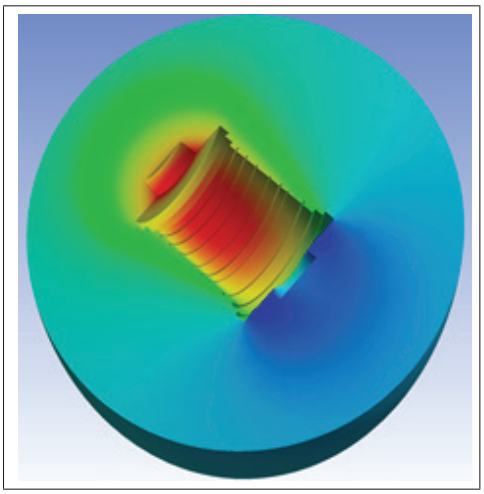

Figure 8. Calculated sound pressure in surrounding air volume of the boat engine for an exemplary frequency.

However, in the context of the coupled approach presented in this paper the following should be noted. Taking a MBS into account, a harmonic analysis is only possible if the shaft displacement describes a recurring orbit, which can occur, for example, at a constant rotational speed, that means for stationary operating points. Otherwise a transient calculation is required. In this case run-up simulations are also possible.

3.3 Validation and Verification of the calculated forces of the coupled approach

As written in section 3.2, for an input current of 300 A and different rotational speeds ($100 - 300\ \frac{rad}{s}$) a resulting torque of $47.2 - 49.5$ Nm was measured. In a magnetostatic analysis 49.6 Nm were calculated using ANSYS. This results in a deviation of the simulation between $0.2 - 5$ % compared to the experimental data. It has to be noted that a magnetostatic analysis does not consider the rotational speed, which explains the range of differences between numerical and experimental results. In addition, that means that the numerical model does not consider eddy currents or other dynamic effects in the magnetostatic case. In contrast, the hysteresis behavior was taken into account in the numerical simulation of the motor, which was used for the comparison mentioned above. However, such hysteresis effects are currently not implemented in our version used for the coupling of the MBS and electrodynamics including feedback. For this reason, the same constant relative permeability is assumed for the stator as for the rotor ($\mu = 4000\ \frac{H}{m}$). If the same setting is used in ANSYS, a torque of 46.3 Nm results, which corresponds to a percentage error of 6.3 % compared to the model with hysteresis. This shows that the hysteresis effects should be taken into account in general. The simulation with our own FE-implementation leads to a torque of 45.6 Nm and thus to a deviation from ANSYS (without hysteresis effects) of $1.5\,\%$. Finally, it can be stated that the presented methodology and model are able to describe the electromagnetic fields and the resulting loads in a suitable way. Table 1 shows the determined torques as well as the maximum vector potential that occur for the different cases.

	Torque $M[Nm]$	Vec. pot. $A[Wb/m]$
Experiment	$47.2 - 49.5$	-
ANSYS with Hys.	49.6	7.11×10^{-3}
ANSYS without Hys.	46.3	7.05×10^{-3}
EMD Electromag.	45.6	6.96×10^{-3}

Table 1. Experimentally and numerically determined torques as well as the maximum vector potential.

3.4 Influence of the coupling of MBS and electrodynamics on the behavior of a generic motor

At this point, a simple motor with one pole pair is used to evaluate the influence of the interactions. For this purpose, in a first step the electrodynamic forces that rotor and stator exert on each other are investigated, when they are in a central position. In a second step the electrodynamic forces are neglected and an eccentric rotor position is studied in the mechanical system while using elastic bearings. The resulting forces in the bearings are examined. In the last step, the two systems are combined and the influence of the coupling is demonstrated. The steps carried out here will be applied in further investigations in the same way to the boat motor. Figure 9 shows the simple motor with FE nodes on the surface of the rotor and stator as well as the corresponding force vectors. Here, a transient calculation with constant rotational speed is carried out. At the interface between rotor and air gap (red dots) or between stator and air gap (blue dots), the electrodynamic forces (arrows) are determined using the Maxwell stress tensor. The time depending node forces are transferred into the frequency domain using a Fast Fourier Transformation (FFT) [11].

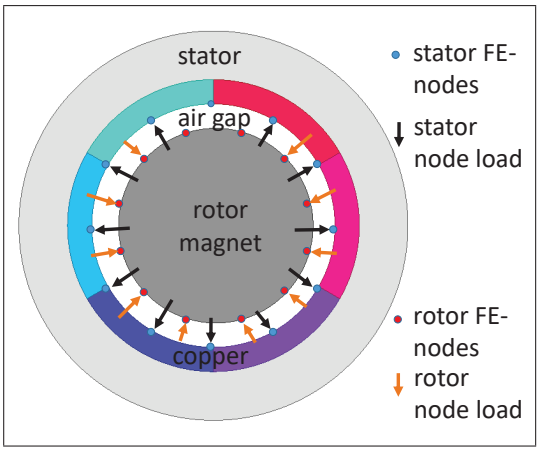

Figure 9. Electrodynamic model of the simple two-pole motor with FE nodes on the surface of the rotor and stator as well as force vectors.

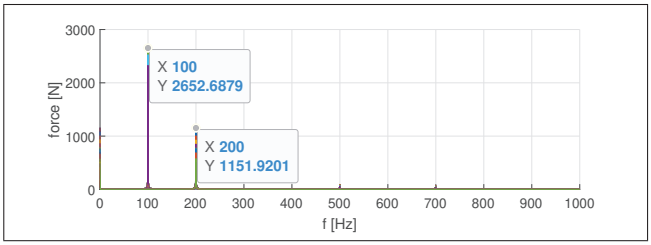

Figure 10. Frequency spectrum of the electrodynamic forces of all FE nodes of the simple motor with the rotor in a central position.

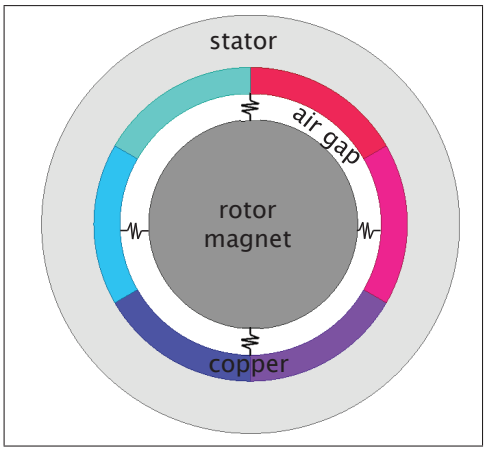

Figure 11. Mechanical model of the simple two-pole motor with elastic bearings without consideration of electrodynamic effects.

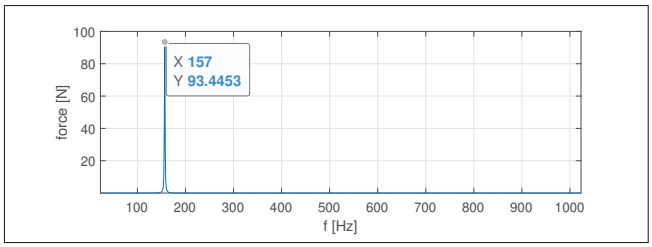

Figure 12. Frequency spectrum of the spring force of the simple motor with elastic bearings and without electrodynamic forces.

This FFT is done for all node forces in the air gap. Figure 10 shows the frequency response of all node forces of the motor at a speed of 100 revolutions per second. In addition to the rotational frequency itself, the double rotational frequency of 200 Hz is clearly visible in Figure 10. This frequency is excited by the two pole pairs. With a 14 −pole motor, e.g. the boat motor presented here, it is expected that a dominant peak at 28 times the speed can be observed.

The air gap is constant for the frequency spectrum shown in Figure 10. This means that the bearings in the motor that are supposed to keep the rotor in the central position of the stator are assumed to be rigid. Now the bearings are represented by springs with a constant spring stiffness of $c = 300 \times 10^3 \ \frac{N}{m}$ each. Figure 11 shows a shaft (rotor $m = 0.62 \ kg$) held in the middle of a bearing block (stator) by springs (bearings). Electrodynamic effects are not taken into account in this model, so that this model is a single-mass oscillator. The corresponding natural frequency ω can be calculated analytically

$$\omega = \sqrt{\frac{2 \cdot c}{m}} \quad . \tag{9}$$

This results in a natural frequency of 157 Hz. As shown in Figure 12, this natural frequency can be confirmed by a FFT of the time signal of the spring forces. For this purpose, a free oscillations test was carried out, i.e. the system was given an initial deflection. The natural frequency determined is independent of the selected initial deflection (except in the static rest position of the system, in which the system is at rest).

Now these two systems will be combined. A transient calculation and a FFT of the calculated node forces is carried out. Both the electrodynamic forces in the motor and the bearing forces (which are approximated by springs) are taken into account. The initial deflection is chosen as in the previous model. The frequency spectrum illustrated in Figure 13 clearly shows the rotational frequency and the double of it. These two frequencies are identical to the ones depicted in Figure 10. The frequency from Figure 12 has been shifted from 157 Hz to 139 Hz. This can be explained with the UMP, which has a similar effect like a spring with negative spring stiffness. Consequently, the overall stiffness is reduced and thus the eigenfrequencies are decreased. Distortion frequencies can be seen in addition to the frequencies shown in Figures 10 and 12 at 61 Hz and 339 Hz. They are the sum or the difference between 200 Hz and 139 Hz. In summary, one of the frequencies has shifted and two new frequencies have been added by considering the coupling between mechanical and electrodynamic system. As a consequence the vibration behavior of the structure has changed. In this minimal example, only the elasticity of the bearings was taken into account. Nevertheless significant influences on the vibration behavior of the overall system were determined. The consideration of shaft deformations, external excitations or other compo-

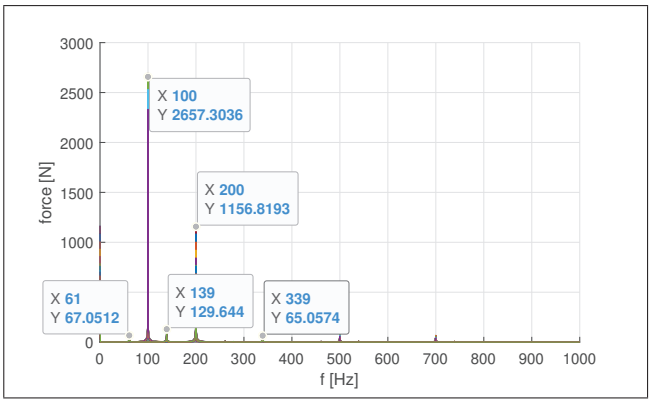

Figure 13. Frequency spectrum of the electrodynamic forces of all FE nodes of the simple motor in the coupled case.

nents also effects the vibration behavior and thus the sound radiation of the electric machine under investigation. This influences will be examined in further work.

4. SUMMARY

A holistic simulation approach is presented, that considers the interactions of structural mechanics and electrodynamics. For this purpose, an existing multi-body program (EMD) was extended to include a FEM force calculation routine for electromagnetic fields. The electrodynamic part separately was validated using experimental data of the boat motor as well as verified by a commercial software (ANSYS). A coupled examination of the motor was carried out, in which the bearings were modeled as elastic elements. The results show that the coupling has a significant influence on the vibration behavior of the system and thus on the emitted sound. In addition to a shift in frequencies, new distortion frequencies appear.

5. OUTLOOK

In further work, the calculation of the electrodynamic forces has to be improved. For this purpose, other influences such as eddy currents and hysteresis effects have to be taken into account. Furthermore, the current two-dimensional FE analyses will be extended to three-dimensional ones. In this way, tilting and deformations of the rotor relative to the stator, which can influence the overall vibration behavior significantly, can be taken into account. The complexity of the included mechanical components will be also increased. In the present work, only elastic bearings are considered in the engine. The aim is to include elastic shafts, external loads and components such as clutches and gears. An experimental validation of the presented coupled approach is planned and already prepared on the required test bench. After the coupling has been implemented and validated successfully, the calculated electrodynamic forces are used to determine their influence on the acoustic behavior of the electric machine. Subsequently different design configurations of the boat motor are compared and evaluated in order to develop an improved prototype from an acoustic point of view (naturally ensuring further auxiliary constrains as minimal mass and required power). The influence of assembly errors or varying current signals will be also investigated.

6. ACKNOWLEDGMENTS

The presented work is part of the joint research project KeM (Kompetenzzentrum eMobility), which is financially supported by the European Union through the European Funds for Regional Development (EFRE) as well as the German State of Saxony-Anhalt (ZS/2018/09/94461). This support is gratefully acknowledged.

7. REFERENCES

[1] A. Tenhunen, "Finite-element calculation of unbalanced magnetic pull and circulating current between parallel windings in induction motor with non-uniform eccentric rotor," *Proceedings of Electromotion*, vol. 1, pp. 19–24, 2001.

[2] M. Wallin, M. Ranlof, and U. Lundin, "Reduction of unbalanced magnetic pull in synchronous machines due to parallel circuits," *IEEE transactions on magnetics*, vol. 47, no. 12, pp. 4827–4833, 2011.

[3] F. Duvigneau, S. Koch, C. Daniel, E. Woschke, and U. Gabbert, "Vibration analysis of an electric wheel hub motor at stationary operating points," in *Proceedings of the 10th International Conference on Rotor Dynamics – IFToMM* (K. Cavalca and H. Weber, eds.), Mechanisms and Machine Science, pp. 51–64, Springer, 2019.

[4] R. Schwertassek and O. Wallrapp, *Dynamik flexibler Mehrkörpersysteme: Methoden der Mechanik zum rechnergestützten Entwurf und zur Analyse mechatronischer Systeme*. Springer-Verlag, 2017.

[5] A. Shabana, *Dynamics of multibody systems*. Cambridge university press, 2020.

[6] J. P. A. Bastos and N. Sadowski, *Electromagnetic modeling by finite element methods*. CRC press, 2003.

[7] D. K. Kalluri, *Advanced Electromagnetic Computation*. CRC Press, 2017.

[8] G. Meunier, *The finite element method for electromagnetic modeling*, vol. 33. John Wiley & Sons, 2010.

[9] J.-M. Jin, *The finite element method in electromagnetics*. John Wiley & Sons, 2015.

[10] M. Schmidt, *Untersuchung charakteristischer Kenngrößen von permanenterregten Synchronmaschinen mit Luftspaltwicklung und messtechnischer Validierung zur Modelloptimierung*. PhD thesis, 2020.

[11] H. J. Nussbaumer, "The fast fourier transform," in *Fast Fourier Transform and Convolution Algorithms*, pp. 80–111, Springer, 1981.